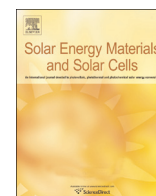




ELSEVIER

Contents lists available at ScienceDirect

Solar Energy Materials & Solar Cells

journal homepage: www.elsevier.com/locate/solmat

Predicting thermal stability of organic solar cells through an easy and fast capacitance measurement

Marta Tessorolo^{a,b}, Antonio Guerrero^{b,*}, Desta Gedefaw^c, Margherita Bolognesi^d, Mario Prosa^a, Xiaofeng Xu^c, Mahdi Mansour^b, Ergang Wang^c, Mirko Seri^{e,*}, Mats R. Andersson^{c,f}, Michele Muccini^a, Germà Garcia-Belmonte^{b,*}

^a Consiglio Nazionale delle Ricerche (CNR), Istituto per lo Studio dei Materiali Nanostrutturati (ISMN), Via P. Gobetti, 101, 40129 Bologna, Italy

^b Institute of Advanced Materials (INAM), Universitat Jaume I, ES-12071 Castelló, Spain

^c Department of Chemistry and Chemical Engineering, Polymer Technology, Chalmers University of Technology, Goteborg SE-412 96, Sweden

^d Laboratory MIST E-R, Via P. Gobetti, 101, 40129 Bologna, Italy

^e Consiglio Nazionale delle Ricerche (CNR), Istituto per la Sintesi Organica e la Fotoreattività (ISOF), Via P. Gobetti, 101, 40129 Bologna, Italy

^f Ian Wark Research Institute, University of South Australia, Mawson Lakes, South Australia 5095, Australia

ARTICLE INFO

Article history:

Received 16 April 2015

Received in revised form

23 May 2015

Accepted 26 May 2015

Keywords:

Thermal stability

Capacitance

Bulk heterojunction

Confocal microscopy

Thermal degradation

Morphological changes

ABSTRACT

Degradation of organic photovoltaic (OPV) devices is currently a topic under intense research as it is one of the main limitations towards the commercialization of this technology. Morphological changes at both active layer and interfaces with the outer contacts are believed to determine main key issues to be overcome. In-line techniques are essential to rule out any effect arising during sample fabrication. Unfortunately, the number of physical techniques able to provide morphological information on complete and operational devices is certainly limited. In this work, we study the thermal degradation of bulk heterojunction (BHJ) solar cells composed by different donor polymers with techniques developed to provide in-situ information on operational devices. Capacitance measurement as a function of temperature monitors the electrical integrity of the active layer and provides the threshold temperature (T_{MAX}) at which the whole device becomes thermally unstable. We found a direct correlation between the threshold temperature T_{MAX} , obtained by capacitance–temperature measurements on complete OPV devices, and the power conversion efficiency decay measured at 85 °C. Devices tend to be thermally stable when the temperature of the thermal stress is below T_{MAX} , while above T_{MAX} evident changes in the active layer or at the active layer/electrode interface are also detected by confocal fluorescence microscopy. The capacitance method gives precious guidelines to predict the thermal stability of BHJ solar cells using an accelerated and easy test.

© 2015 Elsevier B.V. All rights reserved.

1. Introduction

Organic photovoltaic (OPV) devices have to fulfill two fundamental requirements to be competitive in the field of renewable energy sources: (i) power conversion efficiency (PCE) over 10% [1,2] and (ii) lifetime of at least 7–10 years [3]. Recently, laboratory-scale bulk heterojunction (BHJ) solar cells have reached the milestone of 11% [4], through a synergic development of increasingly high performing photoactive materials [5–9], understanding of the morphological film nanostructure [10,11] and device structure optimization [12–18]. Further efficiency improvement is

expected by the use of innovative architectures with improved light absorption such as the use of metasurfaces [19] or layer-by-layer nanoarchitectonics [20]. However, the achievement of high performance has little technological impact if the resulting device lifetime is unsuitable for the technological requirements. For outdoors applications thermal degradation is a key factor that needs to be controlled, as solar panels usually reach temperatures as high as 65–85 °C [21]. Recent studies on several highly efficient OPV devices showed severe efficiency losses even after a short operation time [22]. For this reason, a number of research groups are focused on boosting the lifetime of OPV devices through a deeper study of the degradation mechanisms, attempting to identify, prevent and/or limit them.

Krebs et al. [23] have comprehensively reviewed the most common degradation mechanisms taking place in organic

* Corresponding authors.

E-mail addresses: aguerrer@uji.es (A. Guerrero), mirko.seri@isof.cnr.it (M. Seri), garcia@uji.es (G. Garcia-Belmonte).

photovoltaic. Different physical agents such as humidity, oxygen, UV light and temperature exposure need to be taken into account when studying the degradation of operating OPV devices. Diffusion of water [24] and molecular oxygen [25–27] into the device promotes chemical degradation of interfaces [25] and active material [28]. These effects can be discarded if a device is properly encapsulated. However, degradation pathways due to light soaking and high temperature cannot be eliminated, and, in general, they induce morphology evolution of the active layer [29], interlayer and electrode diffusion [30], and electrode interaction with the organic materials [31]. The behavior of BHJ OPVs after thermal degradation is generally correlated to morphological changes occurring in the active layer that can affect: (i) charge separation process by formation of fullerene aggregates in polymer:fullerene blends, which leads to a PCE loss due to the reduction of the donor:acceptor (D:A) interfacial area [32–34], (ii) charge extraction by a migration of a skin-layer of either polymer [35] or fullerene [36] adhering to the top contact, generating barriers or selective transport regions depending on the device architecture, (iii) transport properties by modification of the polymer packing in the blend [37,38], (iv) recombination by an increase of the number of defect states in the bulk of the active layer [39], and (v) optical properties by generation of a charge transfer complex between donor and acceptor molecules which also acts as an exciton quencher [40]. Several works [33,34] demonstrated that morphological reorganization processes occur only if the solar cell is subjected to temperatures near or above the glass transition temperature (T_g) of the donor polymer. At this temperature devitrification of the blend allows the polymer and the fullerene molecules to rearrange/diffuse in the bulk and at the interface with the electrodes. Typically the T_g of a polymer/blend is measured by Differential Scanning Calorimetry (DSC) [41] but other techniques like ellipsometry have also been employed [38,42]. However, experimental T_g value is not always a well-defined parameter and in many systems a clear transition is not observed. Moreover, this value depends on several aspects such as the thermal history of the sample, the technique/method followed and the thermal rate used for the measurement [43]. For example, recent experiments [44,45] and simulation [46] studies have demonstrated a pronounced thickness-dependent confinement effect on T_g , together with a strong dependence on the solvent and on the substrate used [47]. These effects are totally disregarded if a technique like DSC is employed. On the other hand, ellipsometry can account for this thickness dependence but the presence of the buffer layers and of the electrodes is still not taken into account. In fact, the morphological rearrangement of the BHJ blend which occurs at temperatures above T_g may not be the same in presence or in absence of the top electrode, as demonstrated by several works with the so called “confinement effect” [48]. Taking into account all these considerations, it emerges that it is difficult to predict the thermal behavior of a BHJ solar cell through the bare analysis of the T_g of pristine materials and/or blend films (e.g. measured by DSC or ellipsometry). Indeed, to have a good description of the thermal stability of a solar cell it is crucial to study the properties of the complete device, taking into account the contribution of each layer and each interface on the degradation processes at the same time.

In this work, we study the thermal behavior of different BHJ solar cells using techniques enabling a direct investigation on working devices, such as: (i) current density–voltage characterization to control the evolution of the photovoltaic parameters during the thermal degradation, (ii) capacitance measurements as a function of temperature to monitor the electrical integrity of the active layer, and (iii) fluorescence imaging by Confocal Microscopy to provide visual evidences. Five donor polymers, P(1)-FQ-BDT-4TR, P(2)-PTB7, P(3)-P3HT, P(4)-PTT-MIM, and P(5)-PBnDT-FTAZ

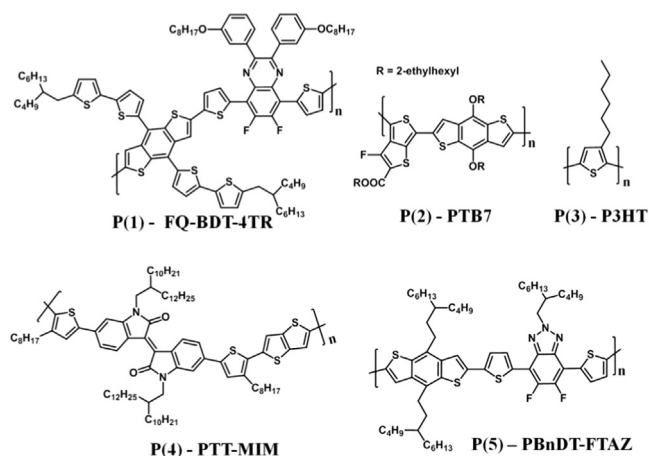


Fig. 1. Chemical structure of the photoactive polymers.

(Fig. 1), which represent a broad range of different types of conjugated polymers, were selected and specific properties of the corresponding BHJ devices were characterized and correlated with the thermal degradation. As a result, we found a direct correlation between the threshold temperature T_{MAX} , obtained by capacitance–temperature measurements on complete OPV devices, and the PCE decay profile measured at 85 °C. In summary, this methodology provides a threshold temperature at which the whole device becomes thermally unstable, thus giving precious guidelines to predict the thermal stability of BHJ solar cells using accelerated tests.

2. Experimental section

For this study we used a standard device architecture: glass/ITO/PEDOT:PSS/Active Layer/ZnO/Ag. The PEDOT:PSS (poly(3,4-ethylenedioxythiophene):poly(4-styrenesulfonate), Clevis P VP A1 4083, H.C Starck) was spun-cast on a pre-cleaned patterned ITO-coated glasses ($R_s \sim 10 \Omega/\square$) to form a thin layer (~ 30 nm) and subsequently annealed at 150 °C for 15 min. Different active layers based on the donor polymers P(1)-FQ-BDT-4TR, P(2)-PTB7, P(3)-P3HT, P(4)-PTT-MIM, and P(5)-PBnDT-FTAZ were prepared. As acceptor materials we used PC₆₁BM ([6,6]-phenyl-C₆₁-butyric acid methyl ester, Solenne BV) or PC₇₁BM ([6,6]-phenyl-C₇₁-butyric acid methyl ester, Solenne BV). The active layers were prepared by spin coating inside the glove-box. The following devices were prepared using recipes reported in literature: P(1):PC₆₁BM (1:1 w/w) [49], P(2):PC₇₁BM (1:1.5 w/w) [12], P(3):PC₆₁BM (1:0.8 w/w) [50] and P(5):PC₆₁BM (1:2 w/w) [51]. On the other hand, P(4):PC₆₁BM (1:1.5 w/w) was deposited from a solution of 1,2-dichlorobenzene and 1,8-Diiodooctane (98:2 v/v) with a total concentration of 30 mg/ml by spinning at 700 rpm for 120 s. Details of the synthesis of P(4) are reported in the [Supporting information](#).

The ZnO (provided by Genes'Ink, Lab'Ink Jet ZnO) was spun cast (inside the glove-box) on the top of the active layer to get a thickness of 50 nm. To complete the device fabrication, Ag (100 nm) was next deposited in high vacuum ($\approx 1 \times 10^{-6}$ Torr) using a thermal evaporator directly connected to the glove-box. The current–voltage (I – V) characteristics of all OPV devices were recorded by a Keithley 236 source-measure unit under simulated AM1.5G illumination of 100 mW/cm² (Abet Technologies Sun 2000 Solar Simulator) inside the glove box. The active area of the devices is 6 mm². The devices were illuminated through a calibrated mask to avoid the parasitic photocurrent arising from the

areas outside the electrodes. The results shown in this work are an average on 6 devices.

The thermal degradation tests were carried out inside the glove-box, by keeping the devices onto a hotplate at 85 °C and measuring them at defined intervals of time, to register the trend of the OPV parameters. The total measurement time under light was shorter than 30 min to avoid the initial burn-in light induced degradation [22].

To determinate the capacitance–temperature dependence, encapsulated devices were measured in an oven in air. Samples were heated at ramp of 1 °C/min from 25 °C to 140 °C and the capacitance was measured every 10 s. Capacitance was measured using a Gamry Instruments Reference 3000 potentiostat/galvanostat/ZRA by applying a small voltage perturbation (20 mV) to guarantee the linearity of the response. The chosen frequency was 10 kHz for P(1), 100 kHz for P(3), 1 kHz for P(2), P(4) and P(5) and the applied voltage was -1 V for each device. These conditions enable monitoring the dielectric capacitance of the active layer. Results shown in this work are an average on 2 representative devices.

Laser scanning confocal fluorescence microscopy (LSCM) was carried out on both freshly prepared and aged devices to monitor the evolution of the active layer morphology with thermal degradation. We used a Nikon TE2000 optical microscope connected with a Nikon EZ-1 confocal scanning head. The laser excitation wavelength was 488 nm. The encapsulated devices were illuminated through the glass/ITO side in the area under the metal electrode. The laser was focused inside the device at a depth corresponding to the active layer and the corresponding confocal photoluminescence signal was collected in reflection mode, through the same optical path of the excitation light. By scanning the samples over a defined area, a two-dimensional map of the photoluminescence intensity is created.

3. Results and discussion

The selection of polymers in this work (Fig. 1) was such to include two of the most widely used donor polymers (P3HT and PTB7) and three other materials synthesized in-house with totally different structural units and different proportion of alkyl chains and branching points [52,53]. Characterization of these polymers by DSC measurements was carried out in two independent

research laboratories (examples are shown in Fig. S1 in Supporting information). Unfortunately, none of the materials provided a clear transition to assign the T_g in the range of temperature considered. This result could be due to the combination of chemical structure and relatively low molecular weight of the materials (reported in Supporting information Table S1), indeed it has been reported that the T_g of P3HT with low molecular weight, is situated at temperatures as low as 12 °C [54]. In addition to the difficulty of interpreting DSC results of pure polymers, it is necessary to consider that after blending with fullerene molecules T_g values might change dramatically [55] by effect of restructuring. Therefore, device thermal stability not only depends on the polymer properties but also on the rest of constituents as discussed in the Introduction. Accordingly, a standard method, as the determination of polymer T_g , cannot be used as a simple guide to predict thermal stability. A range of alternative physical techniques were explored here as next described.

3.1. Lifetime study

All solar cells were fabricated using the same device structure composed by ITO/PEDOT:PSS/Polymer:PCBM/ZnO/Ag. We selected the ZnO/Ag cathode to prevent additional degradation processes, such as oxidation and diffusion, that could occur at the active layer/electrode interface when using other common materials such as Ca/Al [56] or LiF/Al [57]. It should be noted that the initial PCE could be slightly enhanced by further optimizing both the processing conditions and the device stack. However the achievement of “hero” efficiency is out of the aim of this work. Interestingly, a different and/or suboptimal self-organization of the same BHJ active blend affords different PCEs and likely different thermal stabilities of the resulting devices. To this end, our approach can be used for each specific device, independently of the initial PCE, giving an univocal response on its typical thermal resistance. An example of different responses of two P(1) based devices, having different initial PCEs, is reported in the SI (Table S2, Figs. S3 and S4).

The thermal degradation test was performed at 85 °C as a standard temperature [21] and inside the glove-box to prevent interactions of devices with oxygen and/or moisture. The test runs for 20 h and the solar cells were illuminated to monitor the OPV performance for a total period shorter than 30 min, allowing to neglect the initial burn-in light induced degradation [22]. The

Table 1
OPV performance of the different BHJ solar cells, before and after the thermal test.

Donor material	Time (h)	J_{sc} (mA/cm ²)	V_{oc} (V)	FF (%)	PCE (%)	τ^a (h)	PCE_f^a (%)	T_{MAX}^b (°C)
P(1)	0	7.3	0.89	47	3.1	15	92	102
	20	7.5	0.85	46	2.9			
	27	7.5	0.82	46	2.9			
P(2)	0	15.5	0.71	50	5.4	6	57	77
	20	13.5	0.62	39	3.3			
P(3)	0	5.0	0.59	57	1.7	12	29	74
	20	5.2	0.46	34	0.8			
P(4)	0	8.8	0.76	50	3.4	3.5	32	58
	20	7.8	0.51	37	1.5			
P(5)	0	8.3	0.78	44	2.8	0.2	0	53
	0.16	6.8	0.75	36	1.8			

^a Time constant τ and offset PCE_f calculated from PCE decay during the thermal test at 85 °C in glovebox.

^b Value of T_{MAX} obtained from the capacitance vs temperature measurement.

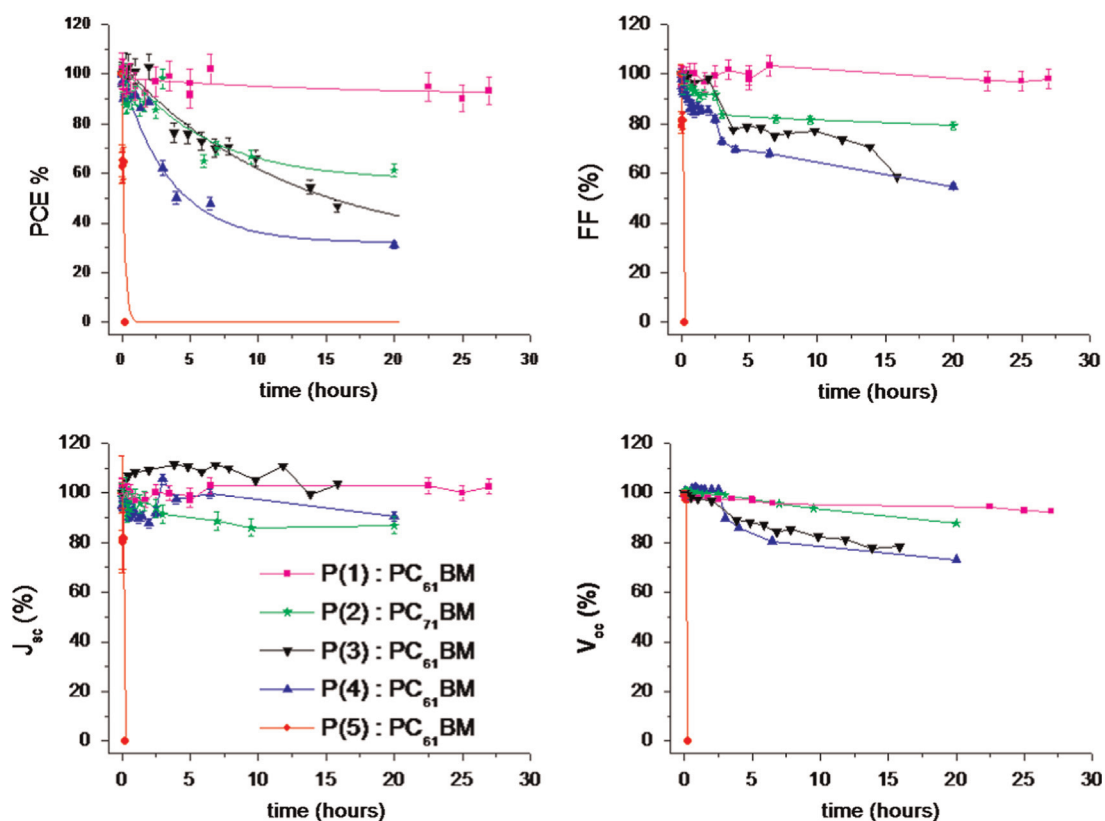


Fig. 2. Evolution with time of the normalized photovoltaic parameters for devices thermally treated at 85 °C in the glovebox.

following degradation effects on the photovoltaic parameters are expected: (i) a reduction of the short circuit current density (J_{sc}) due to morphological changes of the BHJ blend [29,37,38] that can affect the charge mobility and the generation of a charge transfer complex [40]; (ii) a variation of the open circuit voltage (V_{oc}) as a consequence of a different D:A phase segregation [58] and increase of defect states which controls the recombination [39]; and (iii) those phenomena can affect also the fill factor (FF), by a limitation of the charge transport and increase in the series resistance [40].

Table 1 summarizes the OPV response data, before and after thermal degradation, of the different polymer based BHJ solar cells. To better analyze the trend of the OPV performance of each device, normalized PCE, V_{oc} , J_{sc} and FF, as function of time are reported in Fig. 2. Fitting of the PCE data (Fig. 2a) was carried out using an exponential decay: $PCE = PCE_f + (1 - PCE_f) \exp(-t/\tau)$, where t represents the experiment time, PCE_f is the final value attained by the efficiency and accounts for the percentage of the initial efficiency preserved after thermal degradation, while the time constant τ is the lifetime at which the efficiency value is decreased by a factor e , and allows to compare the kinetic of the PCE decay of each sample. The PCE_f and τ values are reported for each device in Table 1.

The most stable device is based on the polymer P(1) as shown in Fig. 2. The drop in normalized PCE is only of 7% after 20 h at 85 °C. For this polymer all the photovoltaic parameters (Fig. 2b–d) remain constant during the experiment time, negligible thermally-induced morphological changes are expected to occur. This result is most probably due to the chemical structure of the polymer with a high proportion of 2D π -conjugated aromatic rings in comparison to the free rotation alkyl chains (Fig. 1) [49]. This configuration allows strong intra- and inter-molecular interactions of the polymer chains which might also hinder the diffusion of the

fullerene molecules, leading to thermodynamically stable thin-film morphology as it will be shown below. In the other extreme, devices fabricated with P(5) degraded very fast: after 1 min of thermal stress PCE drops to 65% of the initial value by the fast initial decay in J_{sc} and FF, leading to a very low efficiency after only 15 min (Fig. 2a). For P(5) important morphological reorganization of the polymer occurs due to the presence of up to three branched alkyl chains in the monomer unit, dramatically reducing the hypothetical T_g . Devices fabricated with the donor polymers P(2)–P(4) show an intermediate behavior between the two extreme cases.

The P(2) based device shows a τ of 6 h and a PCE_f of 57% (Table 1), with a PCE drop from an initial value of 5.4% to a value of 3.3% after 20 h (Table 1). The main factor influencing the degradation trend is FF (Fig. 2b), which drastically decreases due to an increased series resistance in the device, which could be ascribed to a partial segregation between the donor and the acceptor phases within the active layer [37]. This thermally induced reorganization also leads the polymeric chains to rearrange into a morphology with lower charge mobility, as confirmed by the simultaneous decrease of J_{sc} from 15.5 mA/cm² to 13.5 mA/cm² (Fig. 2c). Finally, the P(3) and P(4) based solar cells show similar PCE_f (29% and 32% respectively) but different τ (12 h and 3.5 h, respectively), as shown in Table 1. In the case of P(3), the device shows a constant efficiency during the first 3.5 h of thermal test, while after that time the PCE starts to decrease. As suggested by Bertho et al. in a previous report [34], in the P3HT:PCBM active layer two morphological reorganization processes, with different kinetics, take place. Analogously, in the case of the P(4) based solar cell two degradation mechanisms are occurring: one which affects FF (Fig. 2b) due to an increase in the series resistance in the device, and a second, with a slower kinetic, mostly affecting V_{oc} (Fig. 2d).

3.2. Capacitance vs temperature measurements

To further analyze the thermal response of each polymer-based device we have developed a new method based on the variation of the capacitance as a function of temperature ($C-T$). This method is based on the model proposed by Lungenschmied et al. where the geometrical capacitance (C_g) is used to monitor morphological changes in operating devices [59]. C_g can be expressed by the equation $C_g = \epsilon \epsilon_0 A / L$ where A is the area of the device, L is the thickness of the active layer, ϵ_0 the dielectric constant of vacuum and ϵ the static permittivity of the active layer. When the temperature is increased two phenomena can influence C_g due to significant morphological modification of the active layer: (i) variation of the active layer thickness (L), and (ii) change in the dielectric properties of the blend (ϵ) [60]. To define the conditions at which the C_g should be monitored, we measured the capacitance–voltage characteristics in the dark for each system, from -1 V to 1.5 V at different frequencies. At a certain frequency, typical of each device, the curve has a planar trend in reverse bias, this means that full depletion is achieved in such a way that depletion region covers the whole thickness of the active layer [50]. In this range, the capacitance value corresponds to a geometrical capacitance. (See supporting information Fig. S2 for details). Once selected the correct frequency and applied voltage, devices were introduced in an oven with a heating ramp of 1 °C/min and capacitance was monitored every 10 s. The variation of capacitance with respect to temperature for all P(1)–P(5) based devices is reported in Fig. 3. All the curves have been smoothed and normalized at their maximum to simplify their comparison. A brown dash line at 85 °C indicates the temperature of the standard thermal degradation test described in the previous section. For all devices, except the specific case of P(5), the $C-T$ curve shows an initial rise after which capacitance reaches a maximum value, in correspondence to a temperature defined as T_{MAX} (Table 1), and then starts to decrease. The initial rise is in agreement with previous work on P3HT based devices [42] (P(3)) where the increase in C_g was related to a reduction of the film thickness as a consequence of an increased phase-separation of the BHJ components and possibly to residual solvent loss, resulting in an overall reduction of the free volume of the BHJ films [38]. Moreover Pearson et al. [61] observed that the PEDOT:PSS layer has a thickness contraction in the low temperature range up to 70 °C, which can partially contribute to the initial rise of C_g .

A further increase in the temperature above T_{MAX} gives rise to a capacitance decrease. This fact could be attributed to additional physical or chemical processes occurring in the active layer and/or

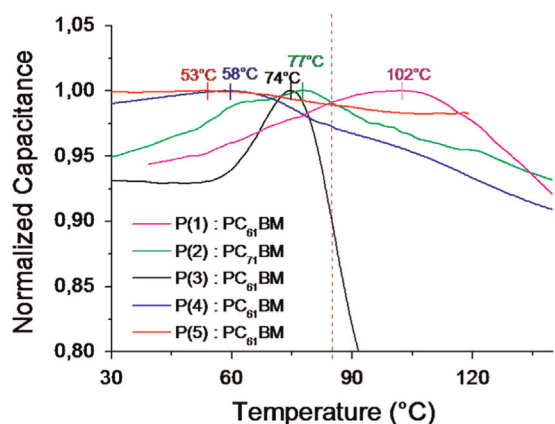


Fig. 3. Normalized capacitance of complete devices thermally treated with a heating ramp of 1 °C/min. The brown dash line indicates the temperature of the thermal life test (85 °C). The maximum of the capacitance–temperature (T_{MAX}) is indicated in the graph for each system.

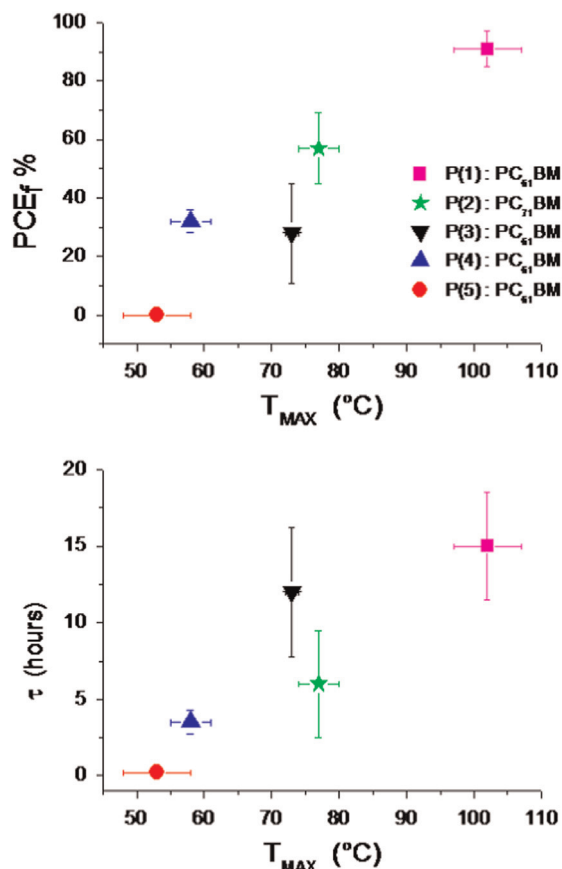


Fig. 4. Correlation between T_{MAX} and parameters extracted from life test at 85 °C: (a) proportion of initial efficiency preservation (PCE_f) after thermal degradation and (b) time constant τ calculated from the PCE decay.

at the active layer/electrode interface which could modify the dielectric permittivity of the layer and/or the thickness of the active layer. To support these hypotheses, a rough theoretical calculation of the expansion coefficient of P(1) based device are reported in the SI (Table S3).

Despite the involved degradation process, the presence of this maximum indicates that significant morphological rearrangements occur in the active blend in relation to the onset of the thermal stability.

The T_{MAX} values extracted from the $C-T$ measurements correlates well with the thermal degradation behavior of the devices observed during the performance thermal tests. Indeed, by plotting the PCE_f and τ values, calculated from the PCE decays during the thermal stress at 85 °C, vs the corresponding T_{MAX} obtained from the $C-T$ measurements (Fig. 4a and b, respectively) for all devices, a clear and direct correlation is found. These findings suggest that T_{MAX} is a good indicator of the thermal stability of a device and it generally represents the operation limiting temperature above which the device becomes thermally unstable.

3.3. Absorption and morphology information

In order to further understand the type of modification leading to device degradation we carried out absorbance measurements (Supporting information, Fig. S5). Measurements were carried out on completed devices before and after the thermal treatment using identical conditions to those used for the capacitance vs temperature measurements. Additionally, measurements on devices thermally treated at 85 °C and 120 °C during 2 h were recorded to understand if longer thermal treatment times lead to

differences in the absorbance spectra. Results suggest that within the level of sensitivity of the technique no significant trends are observed and differences may be due to small batch to batch variations between samples. In any case significant chemical modification of the blends do not appear to be taking place as no significant differences in absorption bands are observed. Therefore, morphological modification seems to be dictating the performance decay.

To explore if morphological changes are taking place with thermal degradation, we need a non-destructive technique that provides morphological information in freshly prepared and aged devices. Laser scanning confocal fluorescence microscopy (LSCM) is a non-invasive technique which allows observing directly the BHJ active layer morphology inside working devices (more details on the measurement are reported in the experimental section). The devices were scanned with a laser at 488 nm and the luminescence signal in the wavelength range 560–700 nm was acquired. At 488 nm light is absorbed only by the donor polymer and the unquenched residual luminescence from the charge generation process and from other minor energy deactivation pathways is monitored. The 2D maps acquired with LSCM represent therefore a projection of the BHJ active layer morphology, where the contrast is determined, within the instrumental resolution, by the different physical and chemical nature of the photoluminescent species in the bulk: domains enriched of donor (D, polymer) would result brighter, while domains enriched of acceptor (A, fullerene) and/or finely intermixed D:A phases would result darker [62]. Confocal fluorescence images of two representative devices based on P(1) and P(3) were recorded first on freshly encapsulated devices, then on the same devices after thermal ageing at 85 °C for 20 h and for 36 h (Fig. 5). These two polymers P(1) and P(3) were selected as they showed T_{MAX} above and below, respectively, the temperature used during the thermal test (85 °C).

The LSCM images registered for the device fabricated with P(1) ($T_{MAX}=102$ °C) reveal a featureless and homogeneous

nanomorphology of the active layer (at the instrumental spatial resolution), which remains stable even after 36 h of thermal stress at 85 °C (Fig. 5a–c). This is in perfect agreement with the nearly unaltered OPV performance of the device reported in Table 1. On the other hand, LSCM images registered for the device fabricated with P(3) (T_{MAX} of 74 °C), which shows a significant decay of the photovoltaic parameters with thermal degradation at 85 °C (Table 1), are reported in Fig. 5d–f. For this device an evident change in the morphology of the BHJ blend is observed after the thermal treatment. Indeed, at time 0 h (Fig. 5a) the morphology is characterized by finely structured intermix of polymer-rich domains (lighter spots) and fullerene-rich domains (darker spots). After 20 h (and even more after 36 h, Fig. 4e and f, respectively) of thermal ageing, a clear reorganization of the blend is observed: the fine structuring of the polymer-rich and fullerene-rich domains disappears concomitantly to the growth of dark spots, which are attributed to fullerene micro-sized aggregates. This is in agreement with the decay of the photovoltaic parameters registered for the P(3) based device during the thermal degradation test at 85 °C (Table 1).

For data completeness, a device fabricated with P(1) was thermally treated at 120 °C, which is a temperature slightly above T_{MAX} . In this case, evident morphological changes of the active layer or at the active layer/electrode interface are observed in the corresponding LSCM map (see Fig. S6 in Supporting information). The lifetime test at 120 °C on the P(1)-based device (Table S4, Fig. S7) indeed revealed a drastic decrease of the photovoltaic performance at this temperature, with a decay time constant (τ) of 0.4 h and an offset PCE_f of 71%.

In summary, whilst a stable nanomorphology is observed for the P(1)-based device treated at a temperature below its T_{MAX} , evident changes in the nanomorphology of the active layer or at the active layer/electrode interface are observed when the P(1) and P(3) based devices are aged at temperatures above their respective T_{MAX} .

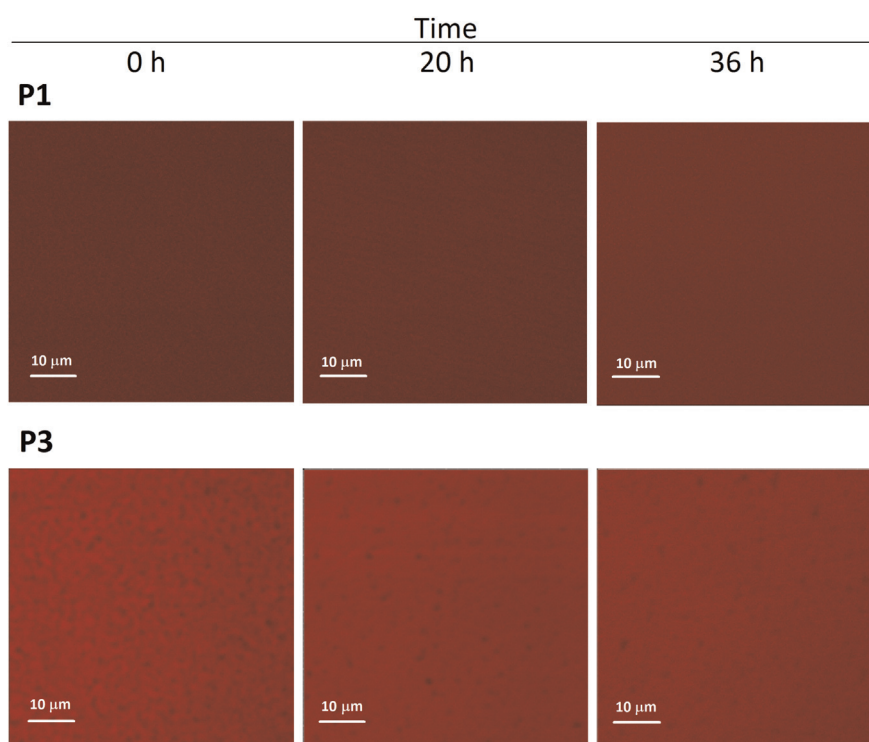


Fig. 5. Confocal fluorescence images of devices thermally treated at 85 °C for different times: P(1) based device after 0 h (a), 20 h (b) and 36 h (c) P(3) based device after 0 h (d), 20 h (e) and 36 h (f) Laser excitation at 488 nm. Images dimension: 50 × 50 μm².

4. Conclusions

In this work we discuss the thermal degradation of organic photovoltaics due to the morphology evolution of the organic layer in complete devices. For this purpose we carried out lifetime tests at 85 °C on a set of five different donor polymers. Degradation data are correlated with other two physical techniques which allow characterization on working devices to account for contact confinement effects. First, capacitance–temperature measurements provide electrical information on the active layer. At a characteristic temperature (T_{MAX}) there is a change in capacitance response which is clearly correlated with the lifetime at a given temperature. As many conjugated polymers do not have a univocal T_g that can be detected by DSC, this technique developed in this work can be a very useful tool and have obvious advantages. On the other hand, laser confocal scanning microscopy provides information on the morphology evolution affecting the active layer and active layer/electrodes interfaces. Whilst stable morphologies are observed for the devices treated at a temperature below T_{MAX} , evident changes in the morphology of the active layer or at the active layer/electrode interface are observed at temperatures above T_{MAX} . The capacitance method presented here constitutes a reliable, fast and easy testing tool to predict the thermal stability of BHJ solar cells.

Acknowledgments

This work was partially supported by FP7 European collaborative project SUNFLOWER (FP7-ICT-2011-7-contract no. 287594), and Generalitat Valenciana, Spain (no. ISIC/2012/008 of Institute of Nanotechnologies for Clean Energies). We further acknowledge Laboratory MIST E-R within the Programma Operativo FESR 2007–2013 of Regione Emilia-Romagna (no. attività I.1.1) for financial support and Vincenzo Ragona for the technical support. The Swedish Research Council was acknowledged for financial support, and Genes'Ink (Marseille, France) for providing ZnO (Lab'Ink Jet ZnO).

Appendix A. Supplementary information

Supplementary data associated with this article can be found in the online version at <http://dx.doi.org/10.1016/j.solmat.2015.05.041>.

References

- [1] G. Dennler, M.C. Scharber, C.J. Brabec, Polymer-fullerene bulk-heterojunction solar cells, *Adv. Mater.* 21 (2009) 1323–1338.
- [2] H.J. Son, B. Carsten, I.H. Jung, L. Yu, Overcoming efficiency challenges in organic solar cells: rational development of conjugated polymers, *Energy Environ. Sci.* 5 (2012) 8158.
- [3] H.-L. Yip, A.K.Y. Jen, Recent advances in solution-processed interfacial materials for efficient and stable polymer solar cells, *Energy Environ. Sci.* 5 (2012) 5994.
- [4] C.-C. Chen, W.-H. Chang, K. Yoshimura, K. Ohya, J. You, J. Gao, Z. Hong, Y. Yang, An efficient triple-junction polymer solar cell having a power conversion efficiency exceeding 11%, *Adv. Mater.* 26 (2014) 5670–5677.
- [5] L. Dou, W.-H. Chang, J. Gao, C.-C. Chen, J. You, Y. Yang, A selenium-substituted low-bandgap polymer with versatile photovoltaic applications, *Adv. Mater.* 25 (2013) 825–831.
- [6] Y.-J. Cheng, S.-H. Yang, C.-S. Hsu, Synthesis of conjugated polymers for organic solar cell applications, *Chem. Rev.* 109 (2009) 5868–5923.
- [7] M. Seri, M. Bolognesi, Z. Chen, S. Lu, W. Koopman, A. Facchetti, M. Muccini, Fine structural tuning of cyanated dithieno[3,2-b:2',3'-d]silole-oligothiophene copolymers: synthesis, characterization, and photovoltaic response, *Macromolecules* 46 (2013) 6419–6430.
- [8] W. Zhuang, M. Bolognesi, M. Seri, P. Henriksson, D. Gedefaw, R. Kroon, M. Jarvid, A. Lundin, E. Wang, M. Muccini, M.R. Andersson, Influence of incorporating different electron-rich thiophene-based units on the photovoltaic properties of isoindigo-based conjugated polymers: an experimental and dft study, *Macromolecules* 46 (2013) 8488–8499.
- [9] M. Tassarolo, D. Gedefaw, M. Bolognesi, F. Liscio, P. Henriksson, W. Zhuang, S. Milita, M. Muccini, E. Wang, M. Seri, M.R. Andersson, Structural tuning of quinoxaline-benzodithiophene copolymers via alkyl side chain manipulation: synthesis, characterization and photovoltaic properties, *J. Mater. Chem. A* 2 (2014) 11162–11170.
- [10] C.R. McNeill, Morphology of all-polymer solar cells, *Energy Environ. Sci.* 5 (2012) 5653.
- [11] M.T. Dang, L. Hirsch, G. Wantz, J.D. Wuest, Controlling the morphology and performance of bulk heterojunctions in solar cells. Lessons learned from the benchmark poly(3-hexylthiophene):[6,6]-phenyl-C61-butyrac acid methyl ester system, *Chem. Rev.* 113 (2013) 3734–3765.
- [12] Z. He, C. Zhong, S. Su, M. Xu, H. Wu, Y. Cao, Enhanced power-conversion efficiency in polymer solar cells using an inverted device structure, *Nat. Photon.* 6 (2012) 591–595.
- [13] S.-H. Liao, H.-J. Jhuo, Y.-S. Cheng, S.-A. Chen, Fullerene derivative-doped zinc oxide nanofilm as the cathode of inverted polymer solar cells with low-bandgap polymer (PTB7-Th) for high performance, *Adv. Mater.* 25 (2013) 4766–4771.
- [14] J. Jo, J.-R. Pouliot, D. Wynands, S.D. Collins, J.Y. Kim, T.L. Nguyen, H.Y. Woo, Y. Sun, M. Leclerc, A.J. Heeger, Enhanced efficiency of single and tandem organic solar cells incorporating a diketopyrrolopyrrole-based low-bandgap polymer by utilizing combined ZnO/polyelectrolyte electron-transport layers, *Adv. Mater.* 25 (2013) 4783–4788.
- [15] M. Bolognesi, M. Tassarolo, T. Posati, M. Nocchetti, V. Benfenati, M. Seri, G. Ruani, M. Muccini, Efficiency enhancement of P3HT:PCBM solar cells containing scattering Zn–Al hydroxalite nanoparticles in the PEDOT:PSS layer, *Org. Photon. Photovolt.* 1 (2013) 1–10.
- [16] N. Zhou, X. Guo, R.P. Ortiz, S. Li, S. Zhang, R.P.H. Chang, A. Facchetti, T.J. Marks, Bithiophene imide and benzodithiophene copolymers for efficient inverted polymer solar cells, *Adv. Mater.* 24 (2012) 2242–2248.
- [17] L. Motiei, Y. Yao, J. Choudhury, H. Yan, T.J. Marks, M.E. van der Boom, A. Facchetti, Self-propagating molecular assemblies as interlayers for efficient inverted bulk-heterojunction solar cells, *J. Am. Chem. Soc.* 132 (2010) 12528–12530.
- [18] M. Prosa, A. Sagnella, T. Posati, M. Tassarolo, M. Bolognesi, S. Cavallini, S. Toffanin, V. Benfenati, M. Seri, G. Ruani, M. Muccini, R. Zamboni, Integration of a silk fibroin based film as a luminescent down-shifting layer in ITO-free organic solar cells, *RSC Adv.* 4 (2014) 44815–44822.
- [19] N. Yu, F. Capasso, Flat optics with designer metasurfaces, *Nat. Mater.* 13 (2014) 139–150.
- [20] K. Ariga, Y. Yamauchi, G. Rydzek, Q. Ji, Y. Yonamine, K.C.W. Wu, J.P. Hill, Layer-by-layer nanoarchitectonics: invention, innovation, and evolution, *Chem. Lett.* 43 (2014) 36–68.
- [21] M.O. Reese, S.A. Gevorgyan, M. Jørgensen, E. Bundgaard, S.R. Kurtz, D.S. Ginley, D.C. Olson, M.T. Lloyd, P. Morvillo, E. Katz, A. Elschner, O. Haillant, T.R. Currier, V. Shrotriya, M. Hermenau, M. Riede, K.R. Kirov, G. Trimmel, T. Rath, O. Inganäs, F. Zhang, M. Andersson, K. Tvingstedt, M. Lira-Cantu, D. Laird, C. McGuinness, S. Gowrisanker, M. Pannone, M. Xiao, J. Hauch, R. Steim, D.M. DeLongchamp, R. Rösch, H. Hoppe, N. Espinosa, A. Urbina, G. Yaman-Uzunoglu, J.-B. Bonekamp, A.J.J.M. van Breemen, C. Girotto, E. Voroshazi, F.C. Krebs, Consensus stability testing protocols for organic photovoltaic materials and devices, *Sol. Energy Mater. Sol. Cells* 95 (2011) 1253–1267.
- [22] C.H. Peters, I.T. Sachs-Quintana, W.R. Mateker, T. Heumueller, J. Rivnay, R. Noriega, Z.M. Beiley, E.T. Hoke, A. Salleo, M.D. McGehee, The mechanism of burn-in loss in a high efficiency polymer solar cell, *Adv. Mater.* 24 (2012) 663–668.
- [23] M. Jørgensen, K. Norrman, F.C. Krebs, Stability/degradation of polymer solar cells, *Sol. Energy Mater. Sol. Cells* 92 (2008) 686–714.
- [24] K. Norrman, S.A. Gevorgyan, F.C. Krebs, Water-induced degradation of polymer solar cells studied by H₂¹⁸O labeling, *ACS Appl. Mater. Interfaces* 1 (2009) 102–112.
- [25] M.O. Reese, A.J. Morfa, M.S. White, N. Kopidakis, S.E. Shaheen, G. Rumbles, D.S. Ginley, Pathways for the degradation of organic photovoltaic P3HT:PCBM based devices, *Sol. Energy Mater. Sol. Cells* 92 (2008) 746–752.
- [26] A. Guerrero, P.P. Boix, L.F. Marchesi, T. Ripolles-Sanchis, E.C. Pereira, G. Garcia-Belmonte, Oxygen doping-induced photogeneration loss in P3HT:PCBM solar cells, *Sol. Energy Mater. Sol. Cells* 100 (2012) 185–191.
- [27] F.C. Krebs, S.A. Gevorgyan, J. Alstrup, A roll-to-roll process to flexible polymer solar cells: model studies, manufacture and operational stability studies, *J. Mater. Chem.* 19 (2009) 5442.
- [28] M. Manceau, A. Rivaton, J.L. Gardette, S. Guillerez, N. Lemaître, The mechanism of photo- and thermooxidation of poly(3-hexylthiophene) (P3HT) reconsidered, *Poly. Degrad. Stab.* 94 (2009) 898–907.
- [29] B. Conings, S. Bertho, K. Vandewal, A. Senes, J. D'Haen, J. Manca, R.A.J. Janssen, Modeling the temperature induced degradation kinetics of the short circuit current in organic bulk heterojunction solar cells, *Appl. Phys. Lett.* 96 (2010) 163301.
- [30] H.J. Kim, H.H. Lee, J.J. Kim, Real time investigation of the interface between a P3HT:PCBM layer and an Al electrode during thermal annealing, *Macromol. Rapid Commun.* 30 (2009) 1269–1273.

- [31] G. Williams, Q. Wang, H. Aziz, The photo-stability of polymer solar cells: contact photo-degradation and the benefits of interfacial layers, *Adv. Funct. Mater.* 23 (2013) 2239–2247.
- [32] J. Vandenberg, B. Conings, S. Bertho, J. Kesters, D. Spoltore, S. Esiner, J. Zhao, G.V. Assche, M.M. Wienk, W. Maes, L. Lutsen, B.V. Mele, R.A.J. Janssen, J. Manca, D.J.M. Vanderzande, Thermal stability of poly[2-methoxy-5-(20-phenylethoxy)-1,4-phenylenevinylene] (MPE-PPV): fullerene bulk heterojunction solar cells, *Macromolecules* 44 (2011) 8470–8478.
- [33] S. Bertho, I. Haeldermans, A. Swinnen, W. Moons, T. Martens, L. Lutsen, D. Vanderzande, J. Manca, A. Senes, A. Bonfiglio, Influence of thermal ageing on the stability of polymer bulk heterojunction solar cells, *Sol. Energy Mater. Sol. Cells* 91 (2007) 385–389.
- [34] S. Bertho, G. Janssen, T.J. Cleij, B. Conings, W. Moons, A. Gadisa, J. D'Haen, E. Goovaerts, L. Lutsen, J. Manca, D. Vanderzande, Effect of temperature on the morphological and photovoltaic stability of bulk heterojunction polymer: fullerene solar cells, *Sol. Energy Mater. Sol. Cells* 92 (2008) 753–760.
- [35] I.T. Sachs-Quintana, T. Heumüller, W.R. Mateker, D.E. Orozco, R. Cheacharoen, S. Sweetnam, C.J. Brabec, M.D. McGehee, Electron barrier formation at the organic-back contact interface is the first step in thermal degradation of polymer solar cells, *Adv. Funct. Mater.* 24 (2014) 3978–3985.
- [36] A. Guerrero, M. Pfannmüller, A. Kovalenko, T.S. Ripolles, H. Heidari, S. Bals, L.-D. Kauffmann, J. Bisquert, G. Garcia-belmonte, Nanoscale mapping by electron energy-loss spectroscopy reveals evolution of organic solar cell contact selectivity, *Org. Electron.* 16 (2015) 227–233.
- [37] I. Cardinaletti, J. Kesters, S. Bertho, B. Conings, F. Piersimoni, J. D'Haen, L. Lutsen, M. Nezladek, B. Van Mele, G. Van Assche, K. Vandewal, A. Salleo, D. Vanderzande, W. Maes, J.V. Manca, Toward bulk heterojunction polymer solar cells with thermally stable active layer morphology, *J. Photon. Energy* 4 (2014) 040997.
- [38] T. Wang, A.J. Pearson, A.D.F. Dunbar, Pa Staniec, D.C. Watters, H. Yi, A.J. Ryan, R.A.L. Jones, A. Iraqi, D.G. Lidzey, Correlating structure with function in thermally annealed PCDTBT:PC70BM photovoltaic blends, *Adv. Funct. Mater.* 22 (2012) 1399–1408.
- [39] T.S. Ripolles, A. Guerrero, G. Garcia-Belmonte, Polymer defect states modulate open-circuit voltage in bulk-heterojunction solar cells, *Appl. Phys. Lett.* 103 (2013) 243306.
- [40] A. Guerrero, H. Heidari, T.S. Ripolles, A. Kovalenko, M. Pfannmüller, S. Bals, L.-D. Kauffmann, J. Bisquert, G. Garcia-Belmonte, Shelf life degradation of bulk heterojunction solar cells: intrinsic evolution of charge transfer complex, *Adv. Energy Mater.* 5 (2014) 1401997. <http://dx.doi.org/10.1002/aenm.201401997>.
- [41] Y. Zhao, G. Yuan, P. Roche, M. Leclerc, A calorimetric study of the phase transitions in poly(3-hexylthiophene), *Polymer* 36 (1995) 2211–2214.
- [42] T. Wang, A.J. Pearson, D.G. Lidzey, R.A.L. Jones, Evolution of structure, optoelectronic properties, and device performance of polythiophene:fullerene solar cells during thermal annealing, *Adv. Funct. Mater.* 21 (2011) 1383–1390.
- [43] M.J. Richardson, N.G. Savill, Derivation of accurate glass transition temperatures by differential scanning calorimetry, *Polymer* 16 (1975) 753–757.
- [44] J.M. Torres, C. Wang, E.B. Coughlin, J.P. Bishop, R.A. Register, R.A. Riggelman, C.M. Sta, B.D. Vogt, Influence of chain stiffness on thermal and mechanical properties of polymer thin films, *Macromolecules* 44 (2011) 9040–9045.
- [45] T. Wang, A.J. Pearson, A.D.F. Dunbar, Pa Staniec, D.C. Watters, D. Coles, H. Yi, A. Iraqi, D.G. Lidzey, R.A.L. Jones, Competition between substrate-mediated π - π stacking and surface-mediated T(g) depression in ultrathin conjugated polymer films, *Eur. Phys. J. E* 35 (2012) 9807, Soft matter.
- [46] A. Shavit, R.A. Riggelman, Influence of backbone rigidity on nanoscale confinement effects in model glass-forming polymers, *Macromolecules* 46 (2013) 5044–5052.
- [47] D. Liu, R. Osuna Orozco, T. Wang, Deviations of the glass transition temperature in amorphous conjugated polymer thin films, *Phys. Rev. E* 88 (2013) 022601.
- [48] X. Yang, A. Alexeev, M.A.J. Michels, J. Loos, Effect of spatial confinement on the morphology evolution of thin poly(p-phenylenevinylene)/methanofullerene composite films, *Macromolecules* 38 (2005) 4289–4295.
- [49] M. Bolognesi, D. Gedefaw, D. Dang, P. Henriksson, W. Zhuang, M. Tassarolo, E. Wang, M. Muccini, M. Seri, M.R. Andersson, 2D π -conjugated benzo[1,2-b:4,5-b']dithiophene- and quinoxaline-based copolymers for photovoltaic applications, *RSC Adv.* 3 (2013) 24543.
- [50] A. Guerrero, L.F. Marchesi, P.P. Boix, S. Ruiz-Raga, T. Ripolles-Sanchis, G. Garcia-Belmonte, J. Bisquert, How the charge-neutrality level of interface states controls energy level alignment in cathode contacts of organic bulk-heterojunction solar cells, *ACS Nano* 6 (2012) 3453–3460.
- [51] S.C. Price, aC. Stuart, L.G. Yang, H.X. Zhou, W. You, Fluorine substituted conjugated polymer of medium bandwidth yield 7% efficiency in polymer-fullerene solar cells, *J. Am. Chem. Soc.* 133 (2011) 4625–4631.
- [52] J. Kesters, S. Kudret, S. Bertho, N. Van Den Brande, M. Defour, B. Van Mele, H. Penxten, L. Lutsen, J. Manca, D. Vanderzande, W. Maes, Enhanced intrinsic stability of the bulk heterojunction active layer blend of polymer solar cells by varying the polymer side chain pattern, *Org. Electron.: Phys. Mater. Appl.* 15 (2014) 549–562.
- [53] S. Bertho, B. Campo, F. Piersimoni, D. Spoltore, J. D'Haen, L. Lutsen, W. Maes, D. Vanderzande, J. Manca, Improved thermal stability of bulk heterojunctions based on side-chain functionalized poly(3-alkylthiophene) copolymers and PCBM, *Sol. Energy Mater. Sol. Cells* 110 (2013) 69–76.
- [54] J. Kesters, S. Kudret, S. Bertho, N. Van den Brande, M. Defour, B. Van Mele, H. Penxten, L. Lutsen, J. Manca, D. Vanderzande, W. Maes, Enhanced intrinsic stability of the bulk heterojunction active layer blend of polymer solar cells by varying the polymer side chain pattern, *Org. Electron.* 15 (2014) 549–562.
- [55] J. Zhao, A. Swinnen, G. Van Assche, J. Manca, D. Vanderzande, B. Van Mele, Phase diagram of P3HT/PCBM blends and its implication for the stability of morphology, *J. Phys. Chem. B* 113 (2009) 1587–1591.
- [56] N. Grossiord, J.M. Kroon, R. Andriessen, P.W.M. Blom, Degradation mechanisms in organic photovoltaic devices, *Org. Electron.* 13 (2012) 432–456.
- [57] D. Liu, T. Nagamori, M. Yabusaki, T. Yasuda, L. Han, K. Marumoto, Dramatic enhancement of fullerene anion formation in polymer solar cells by thermal annealing: direct observation by electron spin resonance, *Appl. Phys. Lett.* 104 (2014) 243903.
- [58] K. Vandewal, S. Himmelberger, A. Salleo, Structural factors that affect the performance of organic bulk heterojunction solar cells, *Macromolecules* 46 (2013) 6379–6387.
- [59] C. Lungenschmied, S. Bauer, R. Schwödauer, S. Rodman, D. Fournier, G. Dennler, C.J. Brabec, Real-time in-situ observation of morphological changes in organic bulk-heterojunction solar cells by means of capacitance measurements, *J. Appl. Phys.* 109 (2011) 044503.
- [60] B. Bernardo, D. Cheyng, B. Verreert, R.D. Schaller, B.P. Rand, N.C. Giebink, Delocalization and dielectric screening of charge transfer states in organic photovoltaic cells, *Nat. Commun.* 5 (2014) 3245.
- [61] A.J. Pearson, T. Wang, R.A.L. Jones, D.G. Lidzey, rationalizing phase transitions with thermal annealing temperatures for P3HT:PCBM organic photovoltaic devices, *Macromolecules* 45 (2012) 1499–1508.
- [62] M. Manceau, A. Rivaton, J.-L. Gardette, S. Guillerez, N. Lemaître, Light-induced degradation of the P3HT-based solar cells active layer, *Sol. Energy Mater. Sol. Cells* 95 (2011) 1315–1325.